ISA Transactions 92 (2019) 118–133

Contents lists available at ScienceDirect

ISA Transactions

journal homepage: www.elsevier.com/locate/isatrans

Research article

Mechanism analysis and suppression strategy research on permanent magnet synchronous generator wind turbine torsional vibration

Jun Liu, Feihang Zhou *, Chencong Zhao, Zhuoran Wang

College of Automation Xi'an University of Technology, China

HIGHLIGHTS

- This paper detailedly analyzed the small signal stability of WECS (wind energy conversion system) based on CMT (Center Manifold Theorem) for the first time.
- The mechanism and reasons of torsional vibration were deeply analyzed and illustrated.
- A damping and stiffness compensation control method was proposed to suppress the torsional vibration.
- Furthermore, this paper provided a complete method for calculating damping and stiffness compensation based on roots locus and bode graph.

ARTICLE INFO

Article history:
Received 29 October 2018
Received in revised form 27 December 2018
Accepted 8 February 2019
Available online 25 February 2019

Keywords:
Torsional vibration
Large-scaled WECS
CMT
DPC

ABSTRACT

Torsional vibration of flexible drive chain is a historical issue. With the maximization development and the rotating machinery high-speed operation, the drive chain systems of large-scaled units become more and more complex, which makes the torsional vibration problems becoming increasingly prominent in recent years. This article deeply analyzed the small signal stability of large-scaled WECS based on CMT, elaborated the torsional vibration mechanism and reasons for the first time and pointed out torsional vibration is caused by the disturbance wind and the DPC strategy. The disturbance wind is an external stimulus and can produce a low-frequency torsional vibration at the same frequency as wind speed. The DPC could weaken the drive chain damping. If the total damping of drive chain is negative, the unstable torsion vibration will occur. And if the drive chain is still a under-damped dynamic, the high-frequency torsional vibration at natural frequency will be generated. Therefore, large-scaled WECS must have damping control. This study found that appropriate enhancing drive chain stiffness could reduce low-frequency torsional vibration caused by wind speed. Therefore, a damping and stiffness compensation control method was proposed to suppress the torsional vibration. Compared with the conventional damping control, the new method not only can suppress the high-frequency torsional vibration but also has a good restraining effect on the low-frequency torsional vibration. Furthermore, the detailed design procedures including the calculation of injection damping and stiffness were given in this paper. Finally, the correctness and effectiveness of our analysis were further verified by the simulation experiments

1. Introduction

In recent years, with the fossil energy sources such as coal, oil and natural gas massively consumed and global climate problem becoming increasingly prominent, the exploration and utilization of renewable energy sources have been paid a high attention to. As the fastest growing renewable energy sources [1–4], wind generation is most prevalent in coastal regions spanning temperate and boreal climates. Furthermore, competing with other renewable energy sources, it is essential to develop the best performance for WT (wind turbine) [5–7]. Meanwhile, the research on wind power has much practical value nowadays. Compared with DFIG (doubly-fed induction generator), PMSG (permanent magnet synchronous generator) with many superior characteristics such as more efficient performance, higher reliability and wider speed control range, is gradually becoming the first choice [8]. Therefore, PMSG-based WECS was selected in this paper.

Over the past 30 years, the size of commercial WTs has exponentially increased from 50 kW in 1980 to 10 MW in 2015 [9]. With the large capacity of single WT and flexible development of the drive chain, the drive chain of WECS will be subjected to a

* Corresponding author.
E-mail address: qq987102679@126.com (F. Zhou).

https://doi.org/10.1016/j.isatra.2019.02.006
0019-0578/

large loads and is more likely to produce torsional vibration. The torsional vibration of WECS is becoming very prominent recently. The wind speed variation and the inappropriate control schemes are the excitation sources of torsional vibration. In general, there are several hazards in torsional vibration:

- In view of the material mechanics, torsional vibration can cause a cyclic alternating stress on the drive chain. Both the amplitude value and frequency of this cyclic alternating stress have an effect on the fatigue life of the drive chain. Therefore, the torsional vibration with large amplitude or high frequency is very harmful to the drive chain.
- Torsional vibration may cause the SSO (sub-synchronous oscillation) problems and WECS will be unstable.
- The 'sub-synchronous frequency components' or 'sub-synchronous harmonics' in electrical parameters such grid-connected voltage and current may be generated at the same frequency as torsional vibration.

For suppressing the torsional vibration of the flexible drive chain, the active damping control of the drive train was illustrated in [10–20]. And this method has been applied to the practical engineering for a long term. Different from the conventional damping control method which needs to extract the torsional vibration information from the generator speed by a band-pass filter, [19] proposed a DC-link current estimation method to obtain the torsional vibration information. [20] further simplified the current estimation method in [19] and pointed out the torsional vibration information could be obtained from the DC-link voltage. Besides, a nonlinear technique based on the sliding mode control theory for torsional vibrations mitigation was proposed in [21] and a virtual inertia control strategy was also put forward in [22]. Meanwhile, there are some ways to suppress the torsional vibration in PMSM (permanent magnet synchronous motor) control. [23,24] carried out a adaptive identification to the torque of drive chain and the load speed based on neural net and the identification values were introduced into the speed control loop and torque control loop as the feedback states. This method has a evident suppression for torsional vibration. [25] proposed a MPC (Model Predictive Control) method and concluded that the MPC has the better suppression effect than the conventional PI control and the PI control based on state feedback mentioned in [26].

The output power command of single WECS must be given by the power divider of wind farm. Actually, the limiting output power condition will occur frequently, whether the wind speed is above the rated wind speed or not. Therefore, limiting output power control is worth researching. As one of the limiting output power control strategies, DPC (direct power control) with a higher response speed and smaller fluctuations for output power can track the power command quickly and has a small impact on the power grid. In view of this, this strategy is adopted in this article. Because of DPC has much more attention to the response speed and small fluctuation of power, it is bound to cause a greater torque impact which is fatal to the flexible drive chain. Therefore, it would be very valuable to study the torsional vibration under DPC.

Based on the above background and problems, this paper has deeply analyzed the mechanism of torsional vibration under DPC and proposed a damping and stiffness compensation control method. Compared with the conventional damping control, the new method has the better torsional vibration suppression. The structure of this paper is as follows: The mathematical model and structure of WECS is briefly introduced in Section 2. Section 3 analyzed the stability of small signal based on CMT. In Section 4, this paper proposed a damping and stiffness compensation control method and gave the detailed design procedure. A simulation test platform based on MATLAB/Simulink simulator was built to verify the effectiveness of the proposed scheme in Section 5. Finally, Section 6 provided some useful conclusions.

2. Mathematical model of WECS

Fig. 1 shows the structure of PMSG based WECS. It is clear that WECS mainly consists of a wind turbine, a flexible chain, a PMSG and power converts.

2.1. Wind turbine model

By the theory of Bates, the aerodynamic power P_{tur} and aerodynamic torque T_{tur} of wind turbine are given by [27,28]

$$P_{tur} = 0.5\pi\rho R^2 C_P v^3 \tag{1a}$$

$$T_{tur} = \frac{P_{tur}}{\omega_{tur}} = 0.5\pi\rho R^3 C_P v^2/\lambda \tag{1b}$$

where ρ is the air density, R is the blade radius, v is the wind speed, ω_{tur} is the wind turbine speed, β is pitch angle, the subscript *tur* refers to the wind turbine and C_P is the wind energy utilization coefficient. λ is TSR (tip speed ratio) and meets

$$\lambda = \frac{R \times \omega_{tur}}{v} \tag{2}$$

In general, C_P is the function β of and λ.

The pitch control is needed under the limiting output power condition. Fig. 2 shows the structure of pitch actuator. It is clear that there is a certain lag between pitch position reference β_{ref} and actual position β.

Eq. (3) could be gotten by Fig. 2.

$$\dot{\beta} = \frac{1}{\tau_\beta}(\beta_{ref} - \beta) \tag{3}$$

where τ_β is the inertia-time-constant of pitch actuator, s is Laplace factor and the subscript *ref* refers to the reference value.

2.2. Flexible drive chain model

For the megawatt PMSG-based WECS, the drive chain bears a heavy load and its flexibility should not be neglected. Therefore, the two-mass–spring–damping model [18–20] was adopted here, shown in Fig. 3.

According to Fig. 3, the mathematical model of flexible drive chain could be described as

$$\begin{pmatrix} J_{tur} & 0 & 0 \\ 0 & J_{gen} & 0 \\ 0 & 0 & 1 \end{pmatrix} \begin{pmatrix} \dot{\omega}_{tur} \\ \dot{\omega}_{gen} \\ \dot{\theta} \end{pmatrix} = \begin{pmatrix} -D & D & -k_s \\ D & -D & k_s \\ 1 & -1 & 0 \end{pmatrix} \begin{pmatrix} \omega_{tur} \\ \omega_{gen} \\ \theta \end{pmatrix} + \begin{pmatrix} 1 & 0 & 0 \\ 0 & -1 & 0 \\ 0 & 0 & 0 \end{pmatrix} \begin{pmatrix} T_{tur} \\ T_{gen} \\ 0 \end{pmatrix} \tag{4}$$

where ω_{gen} is generator speed, T_{gen} is electromagnetic torque, J_{gen} is rotational inertia of generator, θ is shaft twist angle, k_s is stiffness coefficient of flexible drive chain, D is the damping of flexible drive chain and the subscript *gen* refs to the PMSG.

2.3. Dynamic model of PMSG

Actually, the non-salient PMSG dynamic could be considered as a first order inertia link after the inner loop current feedforward decoupling control and the first order tuning for inner loop current PI parameters [29].

$$\varphi(s) = \frac{i_d}{i_{d\_ref}} = \frac{i_q}{i_{q\_ref}} = \frac{T_{gen}}{T_{gen\_ref}} = \frac{1}{\tau_T s + 1} \tag{5}$$

where i_d and i_q are the d-axis and q-axis currents respectively. T_{gen} is the electromagnetic torque. i_{d_ref} and i_{q_ref} are the d-axis and

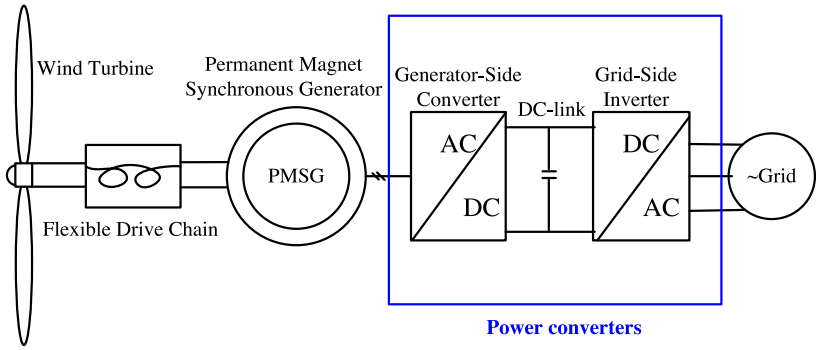

Fig. 1. Structure diagram of WECS.

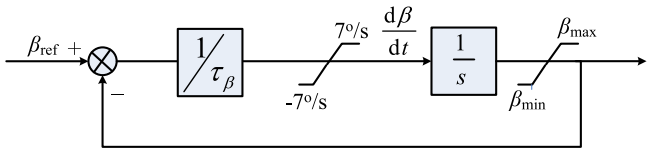

Fig. 2. Structure of pitch actuator.

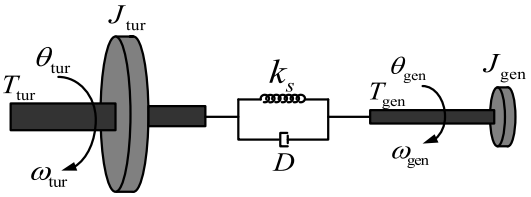

Fig. 3. Two-mass–spring–damping model.

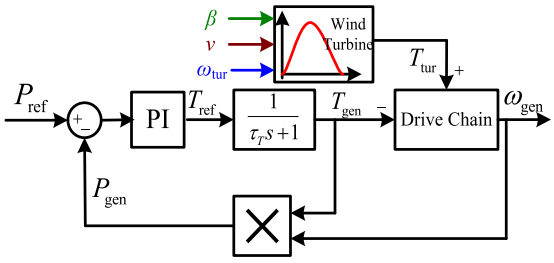

Fig. 4. DPC block diagram.

q-axis currents references. T_{gen_ref} is the electromagnetic torque reference and the inertia-time-constant τ_T meets

$$\tau_T = \frac{R_s}{K_{i\_I}} = \frac{L}{K_{i\_P}} \tag{6}$$

L is the stator-inductances and R_s is the stator-resistance. K_{i_I} and K_{i_P} are the PI parameters of the inner loop current.

3. Small signal stability analysis of WCES

3.1. Small signal model establishment of WECS

First, the aerodynamic torque $T_{tur}(\beta, \omega_{tur}, v)$ in Eq. (1a) is linearized about the operating point.

$$\widetilde{T}_{tur} = a\widetilde{\beta} + b\widetilde{\omega}_{tur} + c\widetilde{v} + o(\widetilde{\beta}, \widetilde{\omega}_{tur}, \widetilde{v}) \tag{7}$$

where the superscript $\sim$ refers the small signal value, the superscript $-$ indicates the mean value and o is higher-order infinitesimal. The aerodynamic factors a, b and c are

$$a = \left.\frac{\partial T_{tur}}{\partial \beta}\right|_{op} = \frac{\rho\pi R^2 \overline{v}^3}{2\overline{\omega}_{tur}} \cdot \frac{\partial C_P}{\partial \beta} \tag{8a}$$

$$b = \left.\frac{\partial T_{tur}}{\partial \omega_{tur}}\right|_{op} = \frac{\rho\pi R^3 \overline{v}^2}{2\overline{\omega}_{tur}} \left(\frac{\partial C_P}{\partial \lambda} - \frac{\overline{C}_P}{\overline{\lambda}}\right) \tag{8b}$$

$$c = \left.\frac{\partial T_{tur}}{\partial v}\right|_{op} = \frac{\rho\pi R^3 \overline{v}}{2} \left(\frac{3\overline{C}_P}{\overline{\lambda}} - \frac{\partial C_P}{\partial \lambda}\right) \tag{8c}$$

Similar to the above analysis, the pitch actuator dynamic could be rewritten as

$$\begin{pmatrix} \dot{\widetilde{\beta}} \\ \dot{\widetilde{\beta}} \end{pmatrix} = \begin{pmatrix} -1/\tau_T & 0 \\ 0 & -1/\tau_T \end{pmatrix} \begin{pmatrix} \widetilde{\beta} \\ \dot{\widetilde{\beta}} \end{pmatrix} + \begin{pmatrix} 0 \\ 1/\tau_T \end{pmatrix} (\beta_{ref}) \tag{9}$$

By linearizing Eq. (4) at the working point, the small signal model of drive chain is

$$\begin{pmatrix} J_{tur} & 0 & 0 \\ 0 & J_{gen} & 0 \\ 0 & 0 & 1 \end{pmatrix} \begin{pmatrix} \dot{\widetilde{\omega}}_{tur} \\ \dot{\widetilde{\omega}}_{gen} \\ \dot{\widetilde{\theta}} \end{pmatrix} = \begin{pmatrix} -D & D & -k_s \\ D & -D & k_s \\ 1 & -1 & 0 \end{pmatrix} \begin{pmatrix} \widetilde{\omega}_{tur} \\ \widetilde{\omega}_{gen} \\ \widetilde{\theta} \end{pmatrix} + \begin{pmatrix} 1 & 0 & 0 \\ 0 & -1 & 0 \\ 0 & 0 & 0 \end{pmatrix} \begin{pmatrix} \widetilde{T}_{tur} \\ \widetilde{T}_{gen} \\ 0 \end{pmatrix} \tag{10}$$

and the slow dynamic of drive chain is

$$\begin{pmatrix} J_{tur} \\ J_{gen} \end{pmatrix} (\dot{\overline{\omega}}) = \begin{pmatrix} -k_s \\ k_s \end{pmatrix} (\overline{\theta}) + \begin{pmatrix} 1 & 0 \\ 0 & -1 \end{pmatrix} \begin{pmatrix} \overline{T}_{tur} \\ \overline{T}_{gen} \end{pmatrix} \tag{11}$$

where $\overline{\omega}$ meets $\overline{\omega} = \overline{\omega}_{tur} = \overline{\omega}_{gen}$. And the above formula Eq. (11) can be further simplified to

$$J\frac{d\overline{\omega}}{dt} = \overline{T}_{tur} - \overline{T}_{gen} \tag{12}$$

where J is the equivalent rotational inertia of system and meets $J = J_{tur} + J_{gen}$.

Fig. 4 depicts the structure diagram of DPC where the PI parameters of the power-outer-loop controller is marked as k_p and k_i.

At this time, the dynamics controller [19] is

$$\widetilde{T}_{gen} = (0 - \overline{T}_{gen}\widetilde{\omega}_{gen} - \overline{\omega}_{gen}\widetilde{T}_{gen} - \widetilde{T}_{gen}\widetilde{\omega}_{gen})\frac{k_p s + k_i}{s(\tau_T s + 1)} \tag{13a}$$

$$\overline{T}_{gen} = (P_{ref} - \overline{T}_{gen}\overline{\omega}_{gen})\frac{k_p s + k_i}{s(\tau_T s + 1)} \tag{13b}$$

By setting $X = (\widetilde{\beta}, \dot{\widetilde{\theta}}, \widetilde{\theta}, \widetilde{\omega}_{tur}, \widetilde{\omega}_{gen}, \widetilde{T}_{gen}, \dot{\widetilde{T}}_{gen})^T$ as the state variables and from Eqs. (7), (9), (10) and (13a), the small signal model of WECS is

$$\dot{X} = AX + Bu + O(X, u) \tag{14}$$

where A, B, $O(X, u)$ and u are in Appendix.

3.2. Small signal stability analysis

Based on the small signal model in Eq. (14), the characteristic polynomial of WECS $m(s)$ is

$$\begin{aligned} m(s) &= |Is - A| \\ &= \left(s + \tfrac{1}{\tau_\beta}\right) \cdot s \left(m_5 s^5 + m_4 s^4 + m_3 s^3 + m_2 s^2 + m_1 s + m_0\right) \\ &= \frac{m_5}{m_0}(s - \lambda_6)(s - \lambda_5)(s - \lambda_4)(s - \lambda_3) \\ &\quad \times (s - \lambda_2)(s - \lambda_1)(s - \lambda_0) \end{aligned} \tag{15}$$

where m_i ($i = 0, 1, \ldots, 5$) is the polynomial coefficients and $m_0 \neq 0$. λ_j ($j = 0, 1, \ldots, 6$) represents the system eigenvalues and it is clear that $\lambda_6 = -1/\tau_\beta$ and $\lambda_5 = 0$. However, due to the aerodynamic factors a and b in matrix A vary with the wind speed, it is difficult to get or judge m_i and λ_j ($j \neq 5, 6$) directly. In reality, this nonlinear system could be considered as a T–S (Takagi–Sugeno) fuzzy system and the T–S fuzzy inference engine provides us with a way to solve this nonlinear problem. The nonlinear system can be fitted by the multiple linear systems.

First of all, 12 linear subsystems are obtained based on the wind speed $v_k = 14$ m/s, 15 m/s, …, 25 m/s where $k = 0, 1, \ldots, 11$. At this time, the matrix A could be expressed as

$$A = (v - v_k)A_k + (v_{k+1} - v)A_{k+1} \qquad v_k \le v \le v_{k+1} \tag{16}$$

Meanwhile, any eigenvalue λ_j also meets this form.

$$\lambda_j = (v - v_k)\lambda_j^k + (v_{k+1} - v)\lambda_j^{k+1} \qquad v_k \le v \le v_{k+1} \tag{17}$$

In the second place, the pitch angle, aerodynamic factors and eigenvalues at the different wind speed v_k should be calculated based on the system parameters shown in appendix and the control parameters $k_i = 1$, $k_p = 0.005$ and $\tau_T = 0.1$. Then, the results were filled in Table 1.

From Eq. (17) and Table 1, we can judge $\lambda_j < 0$ ($j \neq 5$) and $\lambda_5 = 0$. However, we still cannot judge the stability of the system. Therefore, the small signal stability of the system still needs a further analysis.

Consider a non-linear system $\dot{x} = f(x)$. where $f: (\mathbb{Z} \to \mathbb{R}^n)$ is a continuously differentiable and smooth vector field and $\mathbb{Z} \subset \mathbb{R}^n$ is a domain containing the equilibrium points. Linearize the original system $\dot{x} = f(x)$ at a equilibrium point x_0

$$\dot{x} = Ax \tag{18}$$

where A is the Jacobian Matrix and meets

$$A = \left.\frac{\partial f}{\partial x}\right|_{x=x_0}$$

In general, there are three cases in the stability of the original system at the equilibrium point x_0.

Case 1: All the eigenvalues of the Jacobian Matrix A are negative.

Case 2: A has some eigenvalues with positive real parts.

Case 3: A has some eigenvalues with zero real parts and the rest eigenvalues are negative.

Based on the Lyapunov-stability theory, it is easy to judge the stability of the linearized system $\dot{x} = Ax$. In Case 1 and Case 2, the stability of the original system depends on the linearization system. However, the CMT (*Center Manifold Theorem*) has pointed out that the linearized system failed to determine the original system stability in Case 3. At this moment, the stability of the original system near equilibrium point could be determined by the low-order system corresponding to the original system.

For case 3, we assume there are k zero real parts eigenvalues and $m = n$ - k negative eigenvalues in the Jacobian Matrix A. And a similarity transformation P could be always found to transforms A into a block diagonal matrix Λ.

$$PAP^{-1} = \Lambda = \begin{pmatrix} \Lambda_{11} & 0 \\ 0 & \Lambda_{22} \end{pmatrix} \tag{19}$$

where we assume all eigenvalues in Λ_{11} have zero real parts and Λ_{11} is a $k \times k$ matrix. All eigenvalues in Λ_{22} are negative and Λ_{22} is a $m \times m$ matrix. By the similarity transformation

$$\begin{pmatrix} y \\ z \end{pmatrix} = Px;\ y \in \mathbb{R}^k, z \in \mathbb{R}^m \tag{20}$$

the original system could be transformed into

$$\dot{y} = \Lambda_{11} y + g_1(y, z) \tag{21}$$

$$\dot{z} = \Lambda_{22} z + g_2(y, z) \tag{22}$$

where g_1 and g_2 inherit properties of vector field f.

Remark 1. If $z = h(y)$ is an invariant manifold for system Eqs. (21)–(22) and h is smooth, then $z = h(y)$ is called as a center manifold.

Theorem 1. *If the system Eqs. (21) and (22) lies in a center manifold $z = h(y)$, the system motion in center manifold could be described as a kth-order differential equation*

$$\dot{y} = \Lambda_{11} y + g_1(y, h(y)) \tag{23}$$

Meanwhile, the stability of system Eqs. (21) and (22) are determined by the reduced system Eq. (23).

Proof. See pages 305–307 of [30].

Corollary 1. *Given the state variables $x = (x_1, x_2)^T$, the original system could be rewritten as*

$$\dot{x}_1 = f_1(x_1, x_2) \tag{24}$$

$$\dot{x}_2 = f_2(x_1, x_2) \tag{25}$$

where x_1 are the state variables of eigenvalues with zero real parts, x_2 are the state variables of eigenvalues with negative real parts and vector fields f_1 and f_2 meet $f = (f_1, f_2)^T$. The original system can be directly reduced as the low-order system Eq. (25) in stability analysis.

Proof. Because of the similarity transformation P is the homeomorphic transformation, the topological structures of x_1 and y are equivalent.

$$\dot{x}_1 = f_1(x_1, x_2) \Leftrightarrow \dot{y} = \Lambda_{11} y + g_1(y, h(y))$$

This implies the original system $\dot{x} = f(x)$ can be directly reduced as Eq. (25) in stability analysis.

Table 1
Aerodynamic factors and eigenvalues.

Wind speed	Pitch angle	a	b	λ_6	λ_5	λ_4	λ_3	λ_2	λ_1	λ_0
14 m/s	2.27°	−30 583	− 118 882	−0.2	0	−1.05	−7.19−6.15i	−7.19+6.15i	−0.38−97.10i	−0.38+97.10i
15 m/s	4.76°	−42 522	− 141 884	−0.2	0	−1.65	−7.49−5.94i	7.49+5.94i	−0.40−97.10i	−0.40+97.10i
16 m/s	6.97°	−48 660	− 167 273	−0.2	0	−2.31	−7.73−5.63i	−7.73+5.63i	−0.43−97.10i	−0.43+97.10i
17 m/s	8.96°	−54 740	− 194 091	−0.2	0	−3.04	−8.02−5.17i	−8.02+5.17i	−0.45−97.09i	−0.45+97.09i
18 m/s	10.76°	−61 039	− 221 994	−0.2	0	−3.89	−8.27−4.49i	−8.27+4.49i	−0.47−97.09i	−0.47+97.09i
19 m/s	12.44°	−67 714	− 251 524	−0.2	0	−5.19	−8.33−3.27i	−8.33+3.27i	−0.49−97.08i	−0.49+97.08i
20 m/s	13.98°	−74 696	− 281 944	−0.2	0	−10.71	−6.31−2.44i	−6.31+2.44i	−0.52−97.08i	−0.52+97.08i
21 m/s	15.44°	−82 145	− 314 072	−0.2	0	−13.47	−5.71−3.10i	−5.71+3.10i	−0.55−97.07i	−0.55+97.07i
22 m/s	16.73°	−89 691	− 345 483	−0.2	0	−15.47	−5.45−3.44i	−5.45+3.44i	−0.57−97.06i	−0.57+97.06i
23 m/s	17.97°	−97 749	− 378 592	−0.2	0	−17.41	−5.30−3.68i	−5.30+3.68i	−0.60−97.05i	−0.60+97.05i
24 m/s	19.13°	− 106 187	− 412 457	−0.2	0	−19.26	−5.19−3.87i	−5.19+3.87i	−0.62−97.04i	−0.62+97.04i
25 m/s	20.22°	− 115 026	− 447 104	−0.2	0	−21.09	−5.12−4.01i	−5.12+4.01i	−0.65−97.03i	−0.65+97.03i

Because of the eigenvalue λ_5 which is corresponding to the state variable $\tilde{\dot{\theta}}$ is zero and other eigenvalues are negative, the stability of WECS only depends on the reduced system Eq. (26) by the Corollary 1.

$$\tilde{\ddot{\theta}} = -\left(\frac{1}{J_{tur}}+\frac{1}{J_{gen}}\right)k_s\tilde{\theta} - \left(\frac{1}{J_{tur}}+\frac{1}{J_{gen}}\right)D\tilde{\dot{\theta}} + \frac{1}{J_{tur}} \times \left\{a\tilde{\beta} + b\tilde{\omega}_{tur} + c\tilde{v} + o(\tilde{\beta}, \tilde{\omega}_{tur}, \tilde{v})\right\} + \frac{1}{J_{gen}}\tilde{T}_{gen} \tag{26}$$

The inertia moment has the ability to suppress frequency or speed mutation. Hence, compared with the small inertia system, the big inertia system has the lower speed fluctuation. Due to $J_{tur} \gg J_{gen}$, Eq. (27) could be gotten.

$$\tilde{\omega}_{gen} \gg \tilde{\omega}_{tur} \tag{27a}$$

$$\tilde{\dot{\theta}} \approx -\tilde{\omega}_{gen} \tag{27b}$$

If the spindle speed ω_{tur} is used for the pitch control, $\tilde{\omega}_{tur}$ and $\tilde{\beta}$ could be neglected. At this time, we rewrite the reduced system Eq. (26) as

$$\tilde{\ddot{\theta}} + D_m\tilde{\dot{\theta}} + \omega_n\tilde{\theta} \approx \frac{1}{J_{gen}}\tilde{T}_{gen} + \frac{1}{J_{tur}}\{c\tilde{v} + o(\tilde{v})\} \tag{28}$$

where ω_n could be regarded as the natural torsional vibration frequency of drive chain. ω_n and D_m meet $\omega_n = (k_s/J_{tur}+k_s/J_{gen})^{0.5}$ and $D_m = D(1/J_{tur}+1/J_{gen})$. In general, due to

$$\frac{\tilde{T}_{gen}}{\Delta t} \approx \frac{\partial T_{gen}}{\partial t} = \frac{\partial T_{gen}}{\partial\tilde{\theta}}\tilde{\dot{\theta}}$$

where Δt is the infinitesimal of time, Eq. (28) could be further rewritten as

$$\tilde{\ddot{\theta}} + \left(D_m - \frac{\Delta t}{J_{gen}}\frac{\partial T_{gen}}{\partial\tilde{\theta}}\right)\tilde{\dot{\theta}} + \omega_n^2\tilde{\theta} \approx \frac{1}{J_{tur}}\{c\tilde{v} + o(\tilde{v})\} \tag{29}$$

Because of $\overline{\omega}$ has no relation with $\tilde{\theta}$, we have

$$\Delta t\frac{\partial T_{gen}}{\partial\tilde{\theta}} = \frac{\partial T_{gen}}{\partial\omega_{gen}}\cdot\Delta t\frac{\partial(\tilde{\omega}_{gen}+\overline{\omega})}{\partial\tilde{\theta}} = \frac{\partial T_{gen}}{\partial\omega_{gen}}\cdot\frac{\partial\tilde{\omega}_{gen}}{\left(\partial\tilde{\theta}/\Delta t\right)} = \frac{\partial T_{gen}}{\partial\omega_{gen}}\cdot\frac{\partial\tilde{\omega}_{gen}}{\partial\tilde{\theta}} = -\frac{\partial T_{gen}}{\partial\omega_{gen}} \tag{30}$$

From Eqs. (29) and (30), we also can get

$$\tilde{\ddot{\theta}} + \left(D_m + \frac{1}{J_{gen}}\frac{\partial T_{gen}}{\partial\omega_{gen}}\right)\tilde{\dot{\theta}} + \omega_n^2\tilde{\theta} \approx \frac{1}{J_{tur}}\{c\tilde{v} + o(\tilde{v})\} \tag{31}$$

It is clear that the condition for system stability is

$$\frac{\partial T_{gen}}{\partial\omega_{gen}} > -J_{gen}D_m \approx -D \tag{32}$$

Fig. 5 describes the PMSG torque characteristics before and after the injection of damping. Due to $\partial T_{gen}/\partial\omega_{gen} < 0$ in Fig. 5(a) and if the drive chain is lack of the inherent damping D (suppose $D \approx 0$), it is very likely to not meet the system stability condition in Eq. (32). As Fig. 5(b) shows, the injected electrical damping could enhance the stability margin of the system.

4. Analysis and suppression of torsional vibration

4.1. Analysis of torsional vibration

Torsional vibration is the calculation of the influence of the transmission system excitation frequency on the natural frequency, which reflects the danger of resonance and is mainly concerned with the moment of inertia, the torsional stiffness and the system damping. Torsional vibration is highly destructive for the transmission system. A long-term slight torsional vibration can change the twisting stress on transmission chain, increase fatigue damage and reduce its service life. And a short-term severe torsional vibration can cause damage or breakage of drive chain and affect the safe operation. Whilst there is a long history research on the torsional vibration, the early studies were mainly focused on interaction between flexible drive chain and series compensation capacitor on grid-side such as the steam turbine, water turbine, DFIG-based WECS and so on. For PMSG-based WECS, the back-to-back power converters cut off the contact between generator-side control and series compensation capacitor on grid-side. Hence, the PMSG-based WECS torsional vibration is merely caused by the disturbance of wind and generator control. The disturbance of wind is the external excitation source and it can cause the torsional vibration in the form of forced vibration. The generator control affect the damping of the system and maybe cause the unstable torsional vibration.

From Eqs. (13a) and (27b), we can directly get

$$G_{\tilde{T}\tilde{\omega}}(s) = \frac{\tilde{T}_{gen}(s)}{\tilde{\omega}_{gen}(s)} \approx \frac{-\overline{T}_{gen}(k_ps+k_i)}{\tau_Ts^2+(k_p\overline{\omega}+1)s+k_i\overline{\omega}} \tag{33a}$$

$$G_{\tilde{T}\tilde{\theta}}(s) = \frac{\tilde{T}_{gen}(s)}{\tilde{\theta}(s)} \approx -G_{\tilde{T}\tilde{\omega}}(s)\cdot s \tag{33b}$$

Fig. 6 depicts the drive chain structure under DPC. The closed loop transfer function shown in Fig. 6 is given by

$$G_{\tilde{\theta}}(s) = \frac{\tilde{\theta}(s)}{\tilde{\theta}_{ref}(s)} = \frac{b_2s^2+b_1s+b_0}{d_0(s)} \tag{34}$$

where its characteristic polynomial $d_0(s)$ is

$$d_0(s) = a_4s^4 + a_3s^3 + a_2s^2 + a_1s + a_0 \tag{35}$$

and a_0, a_1, a_2, a_3, a_4, b_0, b_1, b_2 are

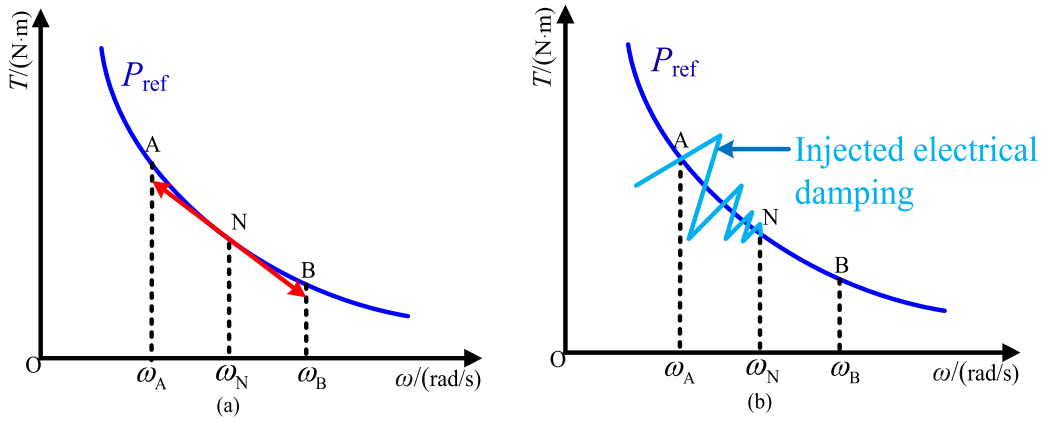

Fig. 5. PMSG torque characteristics under DPC.

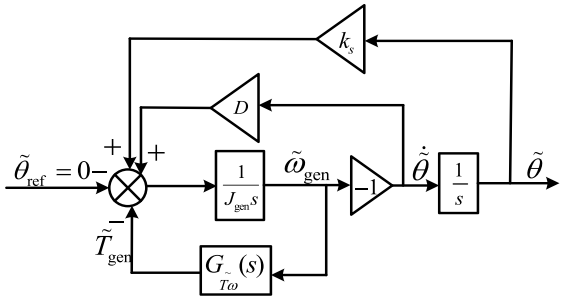

Fig. 6. Structure block of drive chain.

$$
\begin{aligned}
a_0 &= k_i k_s \overline{\omega} \\
a_1 &= k_i D\overline{\omega} + k_p k_s \overline{\omega} + k_s - k_i \overline{T}_{gen} \\
a_2 &= k_p D\overline{\omega} + D + k_i J_{gen}\overline{\omega} + k_s \tau_T - k_p \overline{T}_{gen} \\
a_3 &= k_p J_{gen}\overline{\omega} + J_{gen} + \tau_T D \\
a_4 &= \tau_T J_{gen} \\
b_0 &= k_i \overline{\omega} \\
b_1 &= k_p \overline{\omega} + 1 \\
b_2 &= \tau_T
\end{aligned}
$$

From Eqs. (28) and (33b), the transfer function between disturbance wind and torsional vibration can be described as

$$G_{\widetilde{\theta}\widetilde{v}1}(s) = \frac{\widetilde{\theta}(s)}{\widetilde{v}(s)} \approx \frac{cJ_{gen}}{J_{tur}} G_{\widetilde{\theta}} \tag{36}$$

According to Fig. 6, it is clear that the torsional vibration problem could be regarded as a stabilization problem. The transfer function $G_{\widetilde{T}\widetilde{\omega}}(s)$ called electrical damping is the same as inherent damping D. Due to$G_{\widetilde{T}\widetilde{\omega}}(s) < 0$, this means the power controller can weak the total system damping. If the total damping is negative, the unstable torsional vibration could be induced and the main parameters are oscillatory and divergent. And if the total damping is still weak, the fast oscillatory and slowly convergent torsional vibration could be also activated. The frequencies of these two forms torsional vibration are equal or close to the natural frequency. Besides, Eq. (36) reflects the torsional vibration in the form of forced vibration caused by the disturbance of wind and the frequency of this form torsional vibration only depends on the frequency of wind disturbance.

4.2. Suppression of torsional vibration

(1) *Damping Control Method*

Generally speaking, the damping control has been widely used to suppress the torsional vibration in practical engineering applications and it can enhance the total system damping by injecting electrical damping. The method needs to introduce a compensation torque T_{Comp} corresponding to the injected electrical damping in torque control-loop. In general, the compensation torque T_{Comp} should be assumed as

$$T_{Comp} = k_D \dot{\widetilde{\theta}} \tag{37}$$

where k_D could be considered as the injected electrical damping. At this time, the drive chain structure should be replaced by Fig. 7(a) and the parameters a_1, a_2 and a_3 in Eq. (35) should be changed for

$$
\begin{aligned}
a_1 &= k_i (D + k_D)\overline{\omega} + k_p k_s \overline{\omega} + k_s - k_i \overline{T}_{gen} \\
a_2 &= k_p (D + k_D)\overline{\omega} + D + k_D + k_i J_{gen}\overline{\omega} + k_s \tau_T - k_p \overline{T}_{gen} \\
a_3 &= k_p J_{gen}\overline{\omega} + J_{gen} + \tau_T (D + k_D)
\end{aligned}
$$

As Fig. 7(b) and (c) show, in order to analyze the influence of the injected electrical damping k_D on the system, the root locus of $d_0(s)$ under the change in k_D was gotten where $k_D \in [-4\times10^5, 4\times10^5]$ and the bode diagram of $G_{\widetilde{\theta}}(s)$ also was obtained under k_D takes the different values. The whole calculation process was completed by the MATLAB software under the control parameters and system parameters given in this paper.

By Fig. 7(b), the changes in the system closed-loop eigenvalues λ_i (i = 1, 2, 3, 4) are clear. First, we learned that the change in k_D has little influence on $\lambda_{3,4}$, but it has a great influence on $\lambda_{1,2}$. With the increase of k_D, the real parts of this conjugate complex roots $\lambda_{1,2}$ changed from positive to negative. It should be pointed out here that the stability of system depends on $\lambda_{1,2}$ completely, because the poles $\lambda_{3,4}$ could be offset with zeros $z_{1,2}$ approximately where $\lambda_{3,4} = -4.625 \pm 5.083i$, $z_{1,2} = -5.125 \pm 4.872i$. Hence, $G_{\widetilde{\theta}}(s)$could be simplified as a second-order system shown in Fig. 7(c). As Fig. 7(c) shows, when k_D is over 8.5×10^4, $\lambda_{1,2}$ has a good damping ratio and the resonance point could be completely eliminated. And when k_D is less than 8.5×10^4, the resonance at the drive chain natural frequency 97 rad/s will be excited. Hence, the injected electrical damping must be over 8.5×10^4 at this time.

(2) *Damping and Stiffness Compensation Control method*

The impact of damping on the system is analyzed above. However, what does stiffness have effect on the system? This needs further study. From Eqs. (34) and (35), the static gain of $G_{\widetilde{\theta}}(s)$ is

$$K_G = b_0/a_0 = 1/k_s \tag{38}$$

Eq. (31) indicates that K_G could be reduced by increasing the stiffness. The torsional vibration in the form of forced vibration

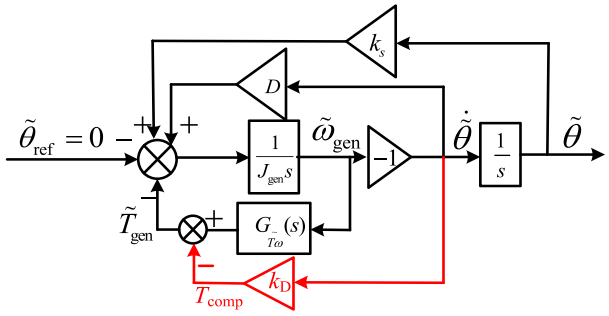

(a) Drive chain structure under the damping control

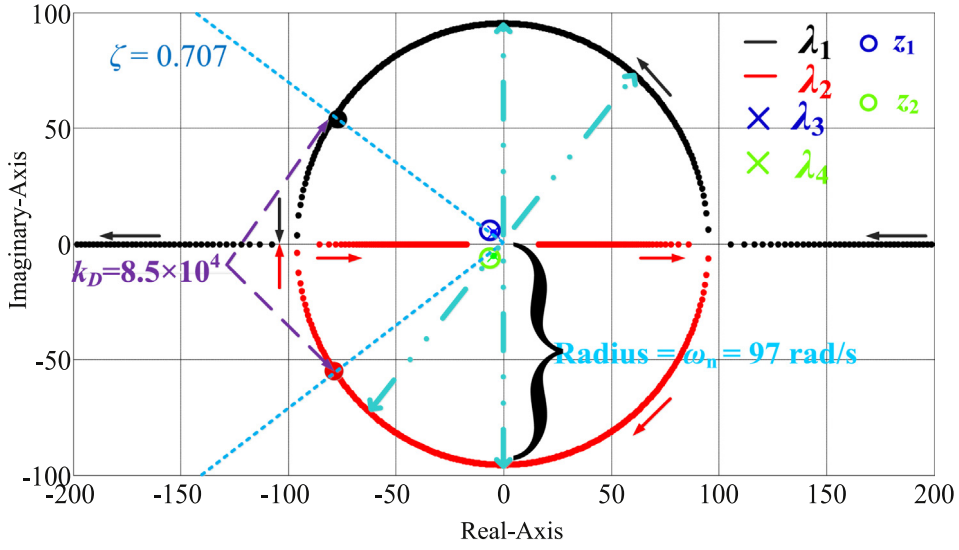

(b) Roots locus of $d_0(s)$

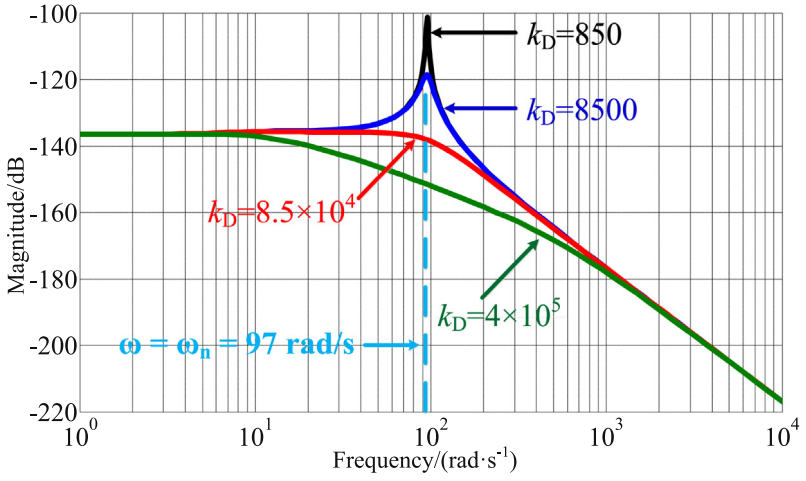

(c) Bode diagram of $G_{\tilde{\theta}}(s)$

Fig. 7. Drive chain structure under the damping control, roots locus of $d_0(s)$ and bode diagram of $G_{\tilde{\theta}}(s)$.

caused by disturbance of wind $\tilde{v}$ including the turbulent wind, the shear wind and the tower-shadow wind could be suppressed by reducing K_G. Certainly, the total stiffness of the system also consist of the inherent mechanical stiffness and the electrical stiffness. Therefore, the anti-disturbance performance of the system can be enhanced by injecting the electrical stiffness. The

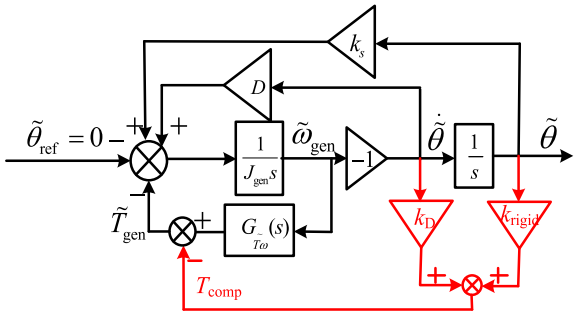

(a) Drive chain structure under the damping and stiffness compensation control

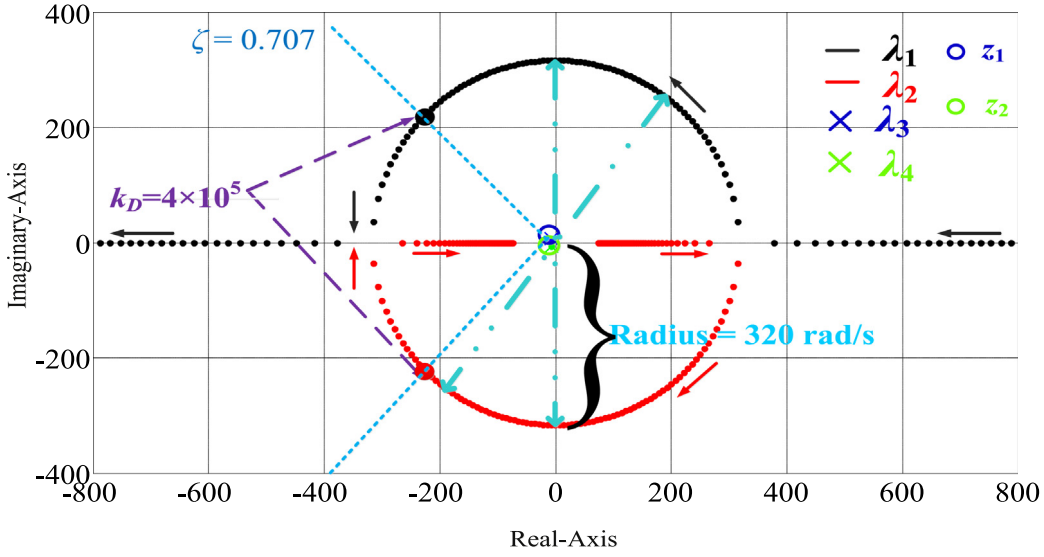

(b) Roots locus of $d_0(s)$

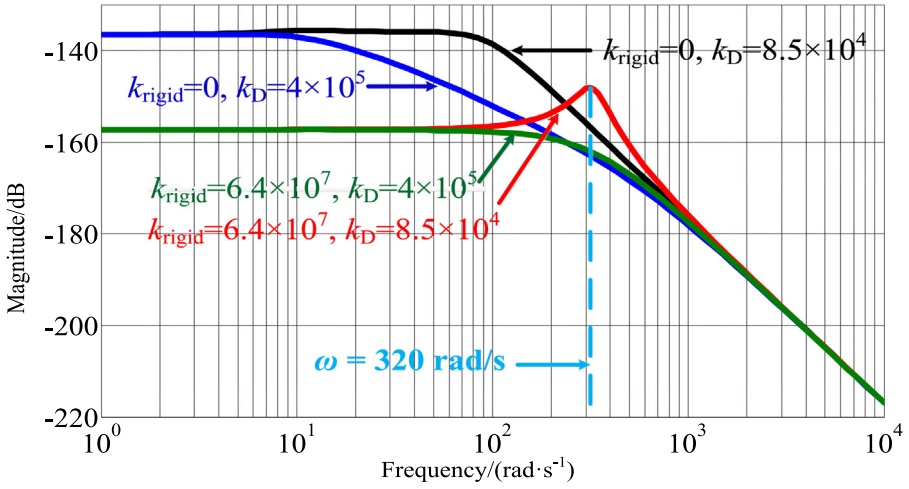

(c) Bode diagram of $G_{\tilde{\theta}}(s)$

Fig. 8. Drive chain structure under the damping control, roots locus of $d_0(s)$ and bode diagram of $G_{\tilde{\theta}}(s)$.

drive chain structure under the damping and stiffness compensation control is shown in Fig. 8(a). If the injected electrical stiffness is remarked as k_{rigid}, the parameters a_0, a_1, a_2 and a_3 in Eq. (35) are changed for

$$a_0 = k_i\left(k_s + k_{rigid}\right)\overline{\omega}$$
$$a_1 = k_i\left(D + k_D\right)\overline{\omega} + k_p\left(k_s + k_{rigid}\right)\overline{\omega} + k_s + k_{rigid} - k_i\overline{T}_{gen}$$

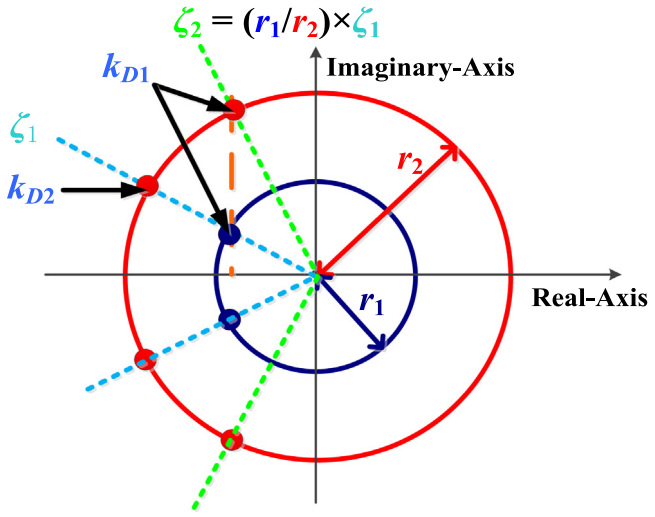

Fig. 9. Roots locus of λ_1 and λ_2.

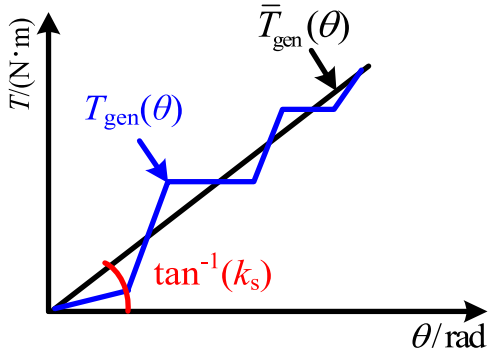

Fig. 10. Relationship between T_{gen} and θ.

$$a_2 = k_p\,(D + k_D)\,\overline{\omega} + D + k_D + k_i J_{gen}\overline{\omega} + \left(k_s + k_{rigid}\right)\tau_T - k_p\overline{T}_{gen}$$
$$a_3 = k_p J_{gen}\overline{\omega} + J_{gen} + \tau_T\,(D + k_D)$$

Given $k_{rigid} = 10k_s$, we also can get the roots locus of $d_0(s)$ under the change in k_D was gotten where $k_D \in [-1\times10^6, 1\times10^6]$, shown in Fig. 8(b). And the bode diagram of $G_{\widetilde{\theta}}(s)$ is shown in Fig. 8(c). By Fig. 8(b), when k_D is over 4×10^5, the system has a good damping for torsional vibration suppression. Fig. 8(c) shows that K_G diminish obviously and the frequency of resonance increase to 320 rad/s, when $k_{rigid} = 6.4\times10^7$ and $k_D = 8.5\times10^4$. At this time, k_D needs the further increase to eliminate the resonance point. When k_D is readjusted to 4×10^5, the new resonance point is completely eliminated.

Injecting the electrical stiffness k_{rigid} can increase the radius of the circle in the roots locus shown in Fig. 9. At this moment, the corresponding damping ratio will decrease. Therefore, it is necessary to continue to increase the electrical damping k_D. Meanwhile, the relationship between the injected damping and stiffness could be calculated by the linear interpolation.

$$\begin{cases} k_D = \dfrac{k_{D2} - k_{D1}}{r_2 - r_1}\,(r - r_1) + k_{D1} \\ r = \sqrt{\left(k_s + k_{rigid}\right)\left(\dfrac{1}{J_{tur}} + \dfrac{1}{J_{gen}}\right)} = \omega_n\sqrt{1 + \dfrac{k_{rigid}}{k_s}} \end{cases}$$

where $kD_1 = 8.5\times10^4$, $kD_2 = 4\times10^5$, $r_1 = 97$ rad/s and $r_2 = 320$ rad/s.

4.3. A way to obtain the torsional vibration information

This paper proposed a new way to obtain the torsional vibration information. In general, $\overline{\theta}$ has nothing to do with $\widetilde{\theta}$ and $\dot{\overline{\omega}}$ where $\overline{\theta} + \widetilde{\theta} = \theta$. From Eq. (11), we can get

$$\frac{\partial\overline{T}_{gen}}{\partial\theta} = \frac{\partial\overline{T}_{gen}}{\partial\overline{\theta}}\cdot\frac{\partial\overline{\theta}}{\partial\theta} = \frac{\partial\overline{T}_{gen}}{\partial\overline{\theta}} = k_s \tag{39a}$$

$$\frac{\partial T_{gen}}{\partial\theta} = \frac{\partial T_{gen}}{\partial\widetilde{\theta}}\cdot\frac{\partial\widetilde{\theta}}{\partial\theta} = \frac{\partial T_{gen}}{\partial\widetilde{\theta}} \tag{39b}$$

As Fig. 10 shows, the relationship between $\overline{T}_{gen}$ and θ is ideal and the ideal curve gradient is k_s by Eq. (39a). The actual relationship between T_{gen} and θ fluctuates on the ideal curve. If the fluctuating bandwidth is smaller, this means the controlling effect is better.

In practice, the spindle speed ω_{tur} and generator speed ω_{gen} usually can be measured directly. Therefore, from Eq. (39a), the torsional vibration information could be given by

$$\begin{cases} \dot{\widetilde{\theta}} = \dot{\theta} - \dot{\overline{\theta}} \approx \dot{\theta} = \omega_{tur} - \omega_{gen} \\ \widetilde{\theta} = \theta - \overline{\theta} \approx \theta - \overline{T}_{gen}/k_s \end{cases} \tag{40}$$

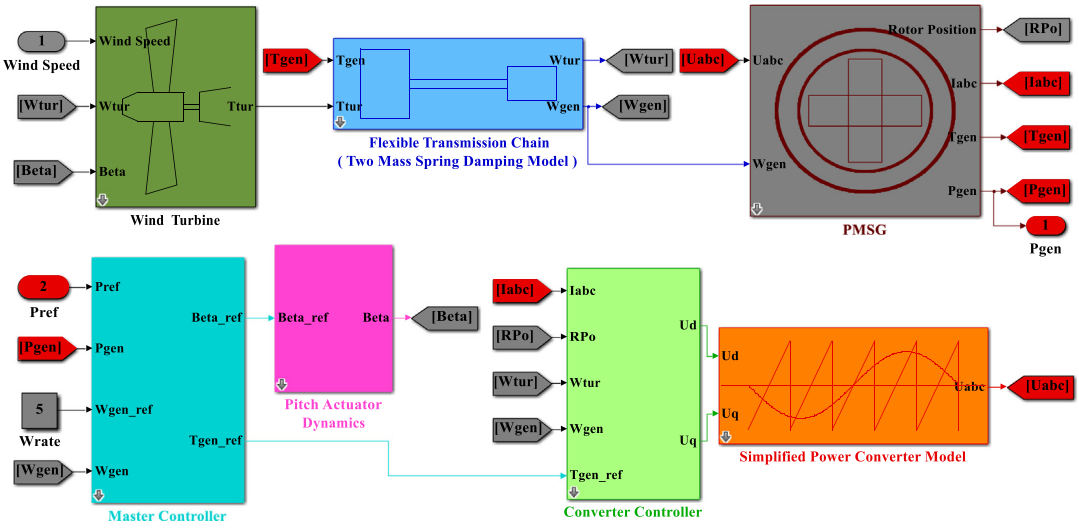

Fig. 11. Simulation test platform.

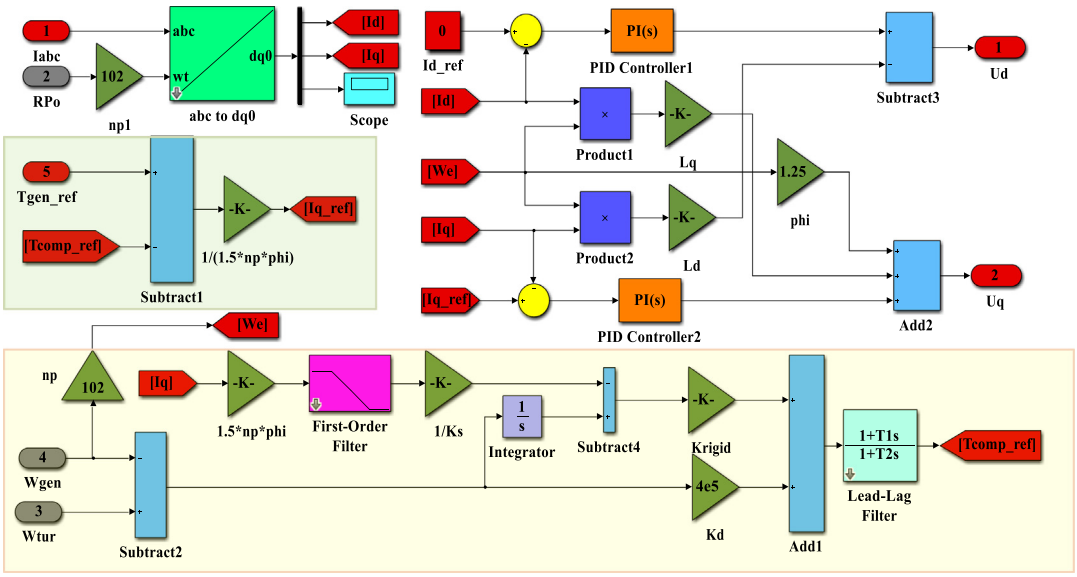

Fig. 12. Algorithm of generator-side converter controller.

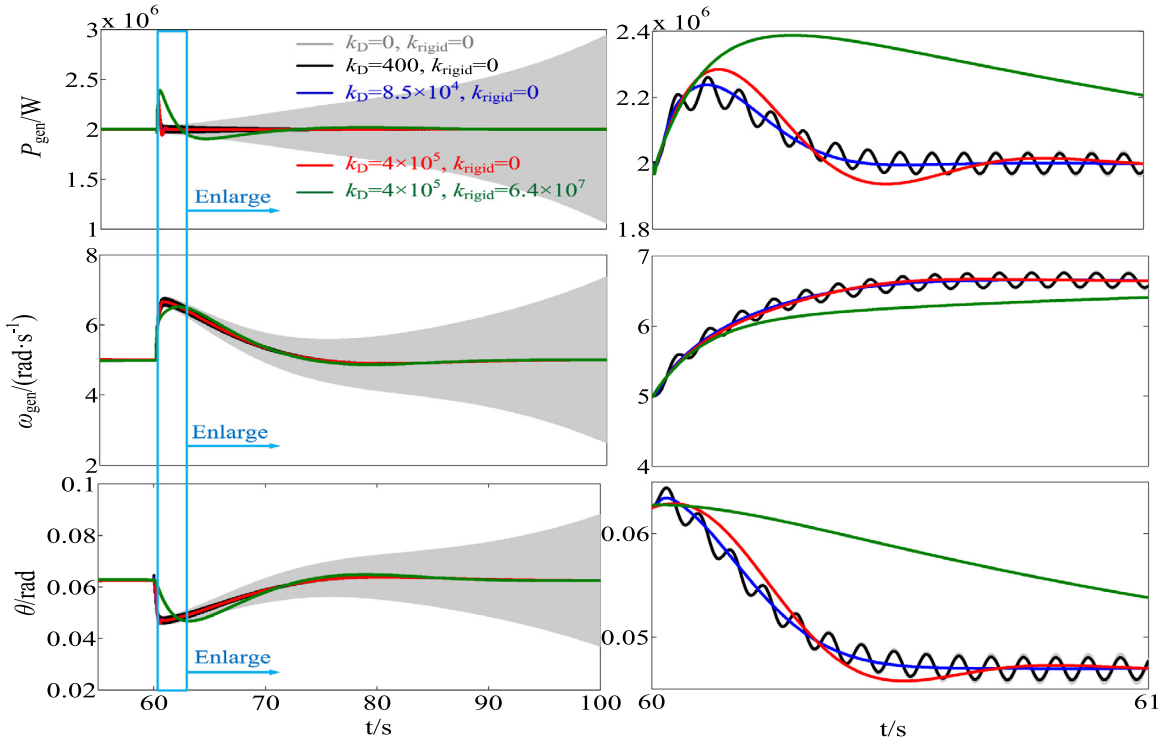

Fig. 13. Responses under the step-wind speed.

5. Analysis and validation of algorithm

In this section, the effectiveness of the algorithms has been validated by a simulation test platform shown in Fig. 11. This simulation test platform based on the Matlab/Simulink environment, is close to the actual physical system and is made up of a wind turbine, a flexible drive chain, a PMSG, a master controller, a pitch actuator dynamic, a converter controller and a simplified power converter model. In reality, the master controller communicates with the converter controller or the pitch actuator dynamic by CANopen or MOUBUS-RTU where the communication delays could be neglected. In general, the torque command and pitch angle command were calculated and sent to the converter controller or the pitch actuator dynamic by the mater controller. The compensation torque T_{comp} must have a higher response to better suppress the torsional vibration. Therefore, T_{comp} should be introduced in the converter controller and the inertia delay of torque Eq. (5) also should be considered. Here, we introduced $G_{\text{comp}}(s)$ to compensate the inertia delay.

$$G_{comp}(s) = \frac{T_{comp\_ref}(s)}{T_{comp}(s)} = \frac{\tau_T s + 1}{\alpha\tau_T s + 1}$$

where T_{comp_ref} is the command of the compensating torque T_{comp} and α meets $0<\alpha<1$. We set $\alpha = 0.01$ here. At this time, the algorithm of the converter controller is shown in Fig. 12.

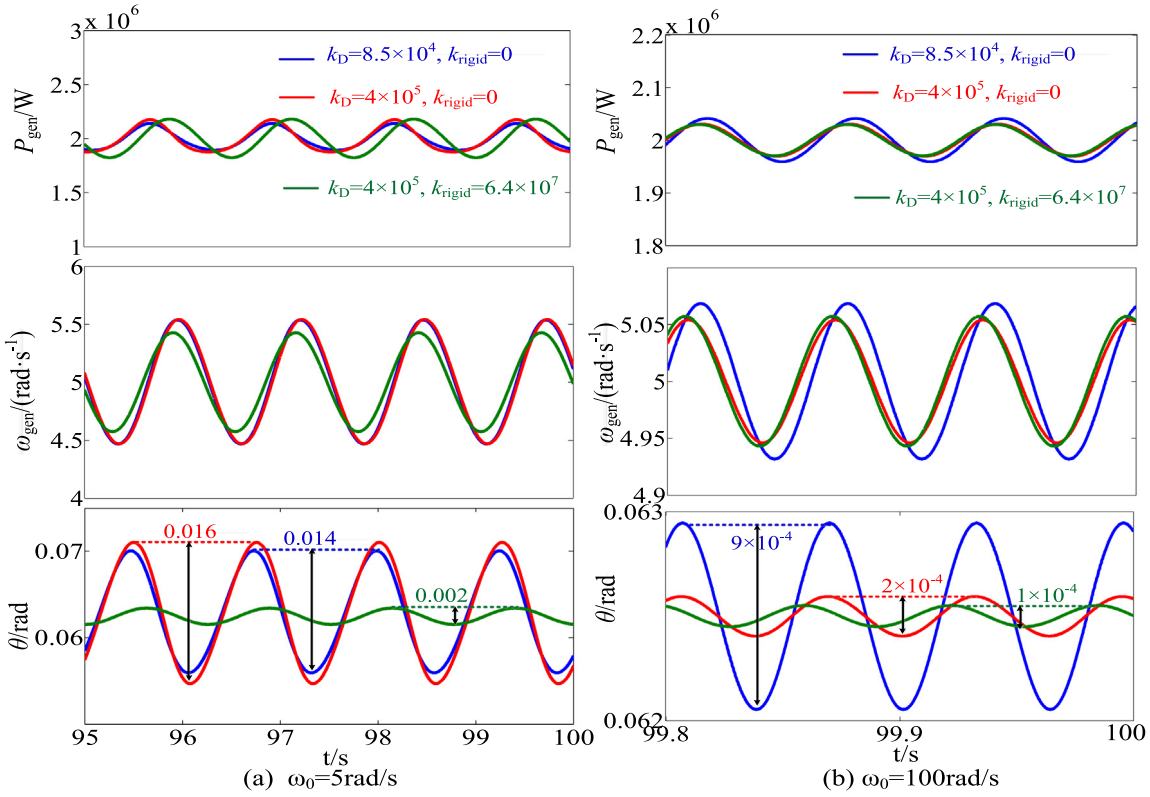

Fig. 14. Responses under the disturbance wind.

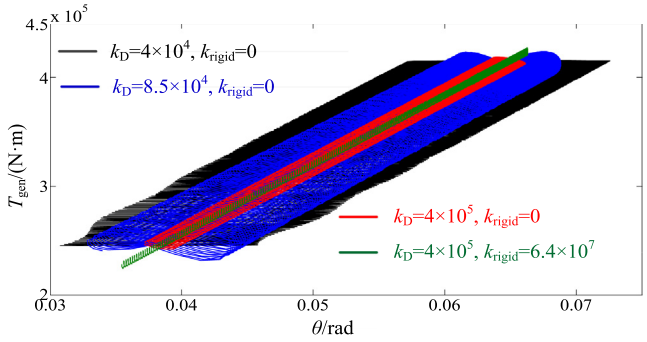

Fig. 15. Relationship between T_{gen} and θ under $\omega_0 = 100$ rad/s.

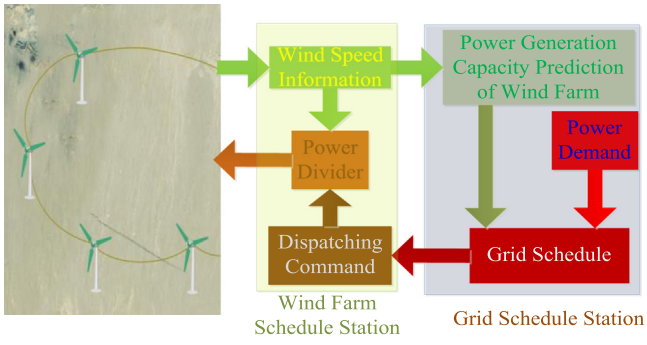

Fig. 16. Distributed control system of wind farm.

5.1. Stability analysis and validation

In order to fully motivate the system, the step-wind was used to simulate the actual wind speed, where the change in wind speed is stepping from 16 m/s to 18 m/s at 60 s in this section. At this moment, the simulation results are shown in Fig. 13.

It is clear that the system without the injected electrical damping k_D will be unstable. With the increase of the injected electrical damping k_D, the stability margin of the system has been improved and the ability to suppress the torsional vibration is also constantly strengthening. When k_D is over 8.5 × 10^4, torsional vibration could be suppressed rapidly. However, the effect of the injected stiffness k_{rigid} on torsional vibration is not yet known in this section. In summary, the system stability is only related to the damping and in order to quickly suppress torsional vibration, it is necessary to continue to increase the damping.

5.2. Torsional vibration suppression in the form of forced vibration

In this section, the torsional vibration suppression in the form of forced vibration was mainly considered. Because of the disturbance wind is the excitation source of this form torsional vibration, the frequency of the torsional vibration entirely depends on the frequency of the disturbance wind. In fact, the disturbance wind should consist of the turbulent wind, the random wind, the shear wind and the tower shade wind. Hence, the disturbance wind should cover multiple frequencies. Although we know the increasing damping is effective for suppressing the torsional vibration, the suppression of the low-frequency torsional vibration and the high-frequency torsional vibration needs to considered separately. At this time, we assume the wind speed is

$$v = v_b + \sin \omega_0 t$$

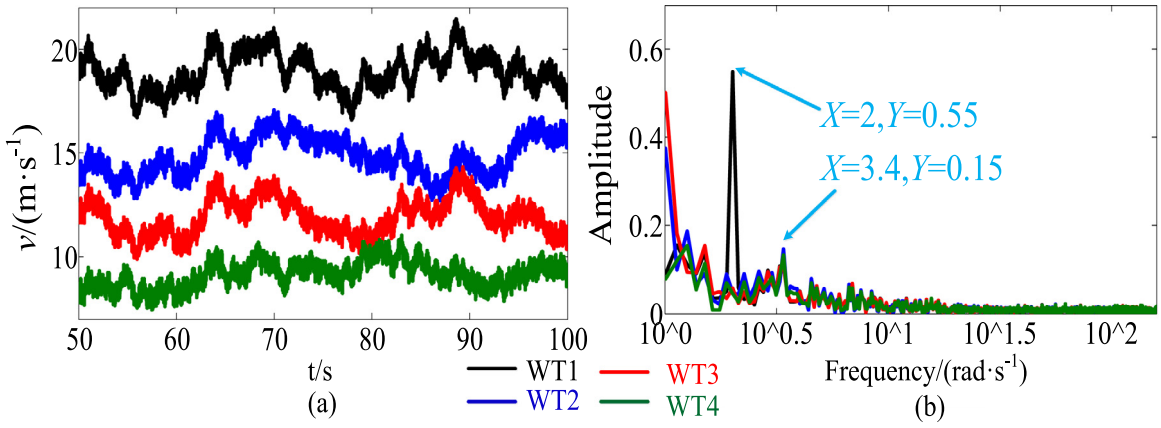

Fig. 17. Wind speeds of WTs.

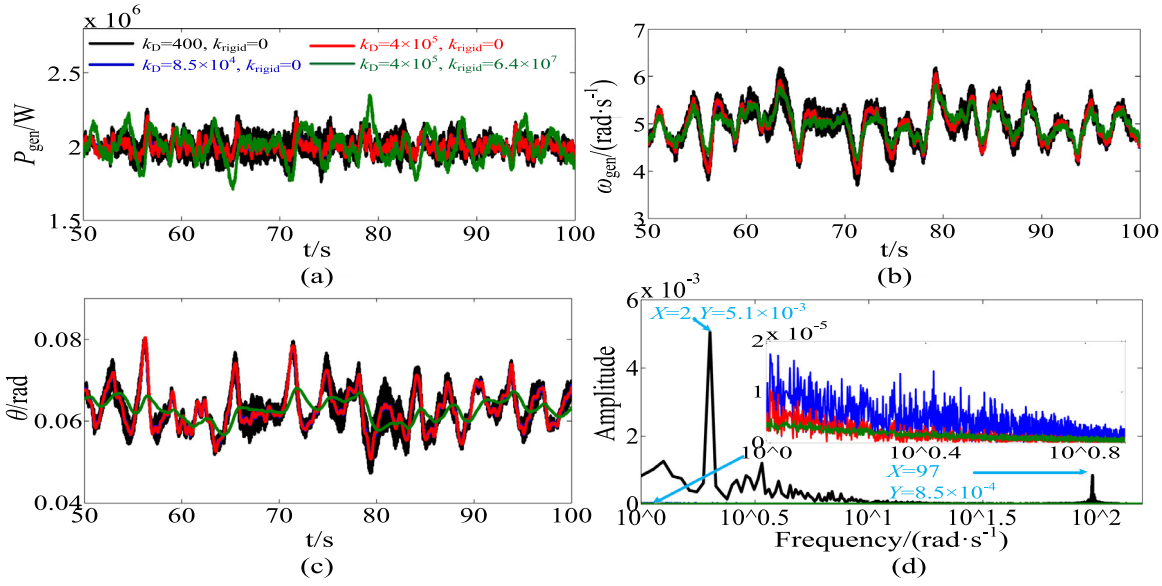

Fig. 18. Responses of WT1.

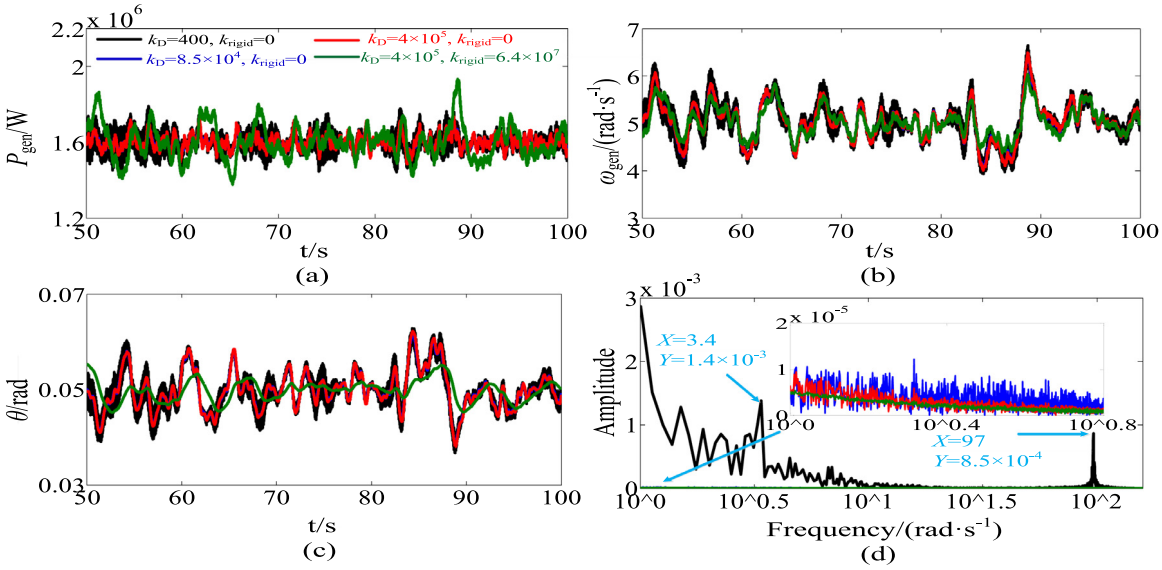

Fig. 19. Responses of WT2.

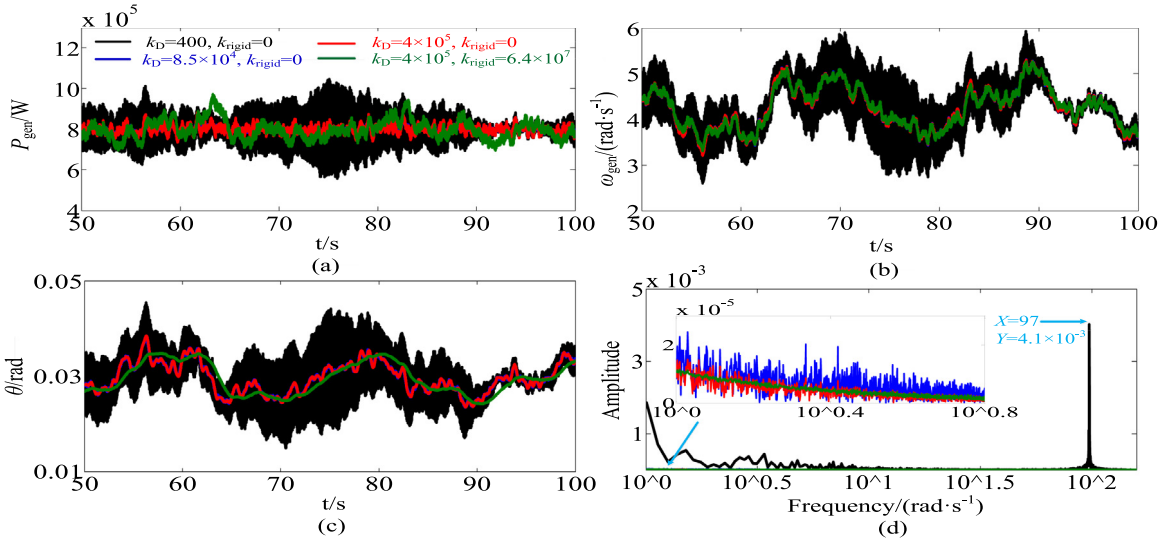

Fig. 20. Responses of WT3.

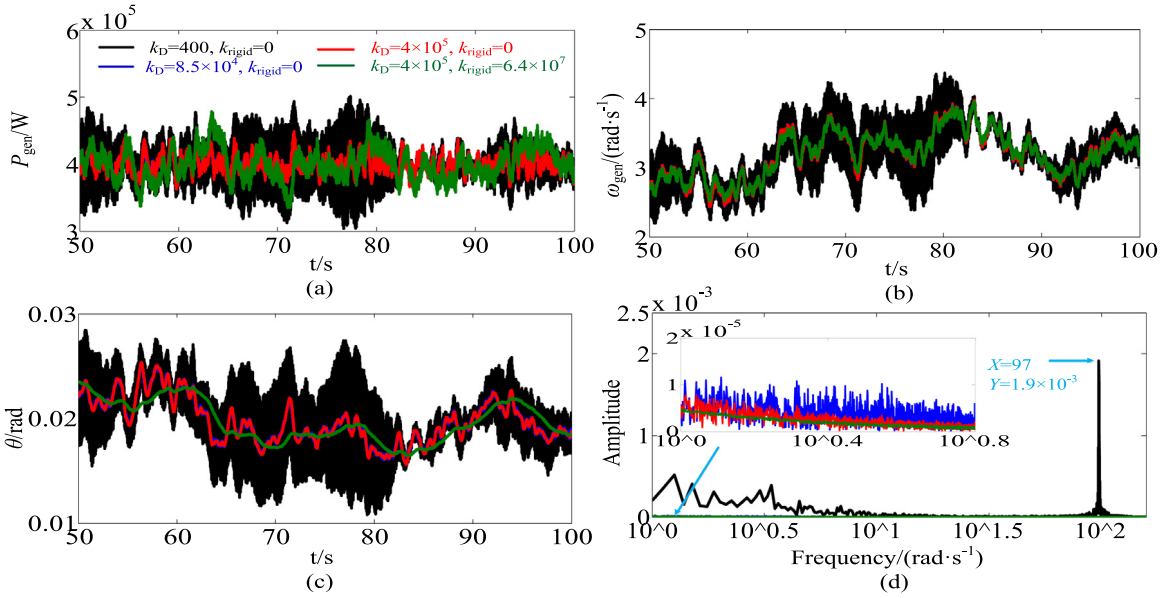

Fig. 21. Responses of WT4.

where v_b is the fundamental wind speed, ω_0 is the frequency of the disturbance wind. In this paper, v_b is chosen as 18 m/s, and ω_0 is chosen as 5 rad/s and 100 rad/s. Then, the simulation results are shown in Fig. 14.

Obviously, further enhancing the damping is still useful for the high-frequency torsional vibration suppression. However, this almost useless for suppressing the low-frequency torsional vibration. At this moment, if we consider the injected stiffness, both the low-frequency and the high-frequency torsional vibration were improved furtherly. Hence, in this section, the effect of the injected stiffness k_{rigid} on the torsional vibration in the form of forced vibration was clear by Fig. 14. As Fig. 15 shows, the fluctuation under the damping and stiffness compensation control is smallest. This means the damping and stiffness compensation control method is best for suppressing this form torsional vibration.

5.3. Torsional vibration suppression in wind turbines

For a further study, we generalized these analyses to other general limiting output power condition. In this section, we suppose that there is a wind farm with four WTs (wind turbines) where the distributed control system of this wind farm is schematically depicted in Fig. 16. Meanwhile, the wind speeds of WTs and the frequency spectrum of wind speeds are shown in Fig. 17. We assumed that the total power dispatching instructions which was given to wind farm schedule station by grid schedule station, was $2.4P_N$ and the wind farm schedule station assigned P_N, $0.8P_N$, $0.4P_N$ and $0.2P_N$ to WT1, WT2, WT3 and WT4 by the wind speeds. The responses of WTs are shown in Figs. 18–21.

Figs. 18(a)–21(a) show the power curves. It is clear that all of the actual power can track power instructions. And the generator speed and torsion angle are shown in Figs. 18(b)–21(b) and

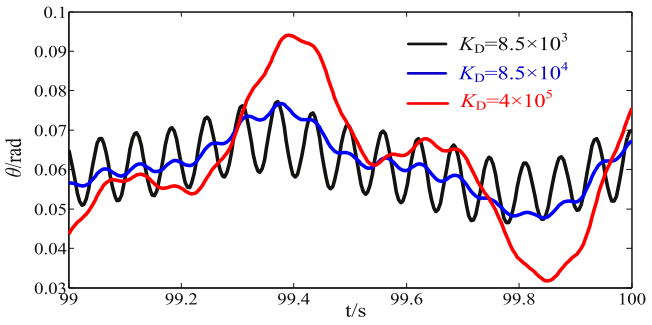

Fig. 22. Torsion angle curves under conventional control method.

Table 2
Bandpass filter parameters.

Symbol	ζ	Ω_0	BW
Value	5	97	154.3804
Unit	–	rad s^{-1}	dec

Figs. 18(c)–21(c). Obviously, the fluctuations of power, generator speed and torsion angle under underdamping is very large. Figs. 18(d)–21(d) are the frequency spectrum of torsion angle θ. From Figs. 18(d)–21(d), we can explain the results more clearly. The results show if the damping is not enough, not only the forced vibration could not be suppressed but also the resonance in the drive chain natural frequency also could be excited. Furthermore, it is evident that the ability to suppress torsional vibration could be furtherly improved by simultaneously injecting the damping and stiffness.

5.4. Comparisons with the conventional method

In this section, the effectiveness and superiority of proposed method is further verified by comparing with the conventional method mentioned in [10–18]. The conventional method obtains the torsional vibration information from generator speed by a bandpass filter. And the compensating torque in conventional method is

$$\begin{cases} T_{comp} = K_D H(s)\omega_{gen} \\ H(s) = \dfrac{2\zeta s/\Omega_0}{s^2/\Omega_0^2 + 2\zeta s/\Omega_0 + 1} \end{cases}$$

where K_D is the injected damping, $H(s)$ is the transfer function of bandpass filter, s is the Laplace variable, ζ is the damping ratio and Ω_0 is the center frequency of bandpass filter (in general, Ω_0 meets $\Omega_0 = \omega_n$). The values of these parameters in are shown in Table 2. Meanwhile, the bandwidth BW of the bandpass filter is given by

$$BW = \frac{\zeta \Omega_0}{\pi}.$$

The simulation test aims to compare and evaluate the performance of this two suppression strategies at the variable wind speed

$$v = 18 + \sin(5t) + \sin(10t) + \sin(20t) + 2\sin(100t) + \mathrm{rand}(t)$$

Firstly, for the conventional control method, it still needs to determine the value of the injected damping K_D. Fig. 22 shows the torsion angle curves with different values of K_D under conventional control method. Obviously, torsional vibration at the natural frequency of the drive chain is still intense with $K_D = 8.5 \times 10^3$. On the contrary, when K_D increases to 4×10^5, although the torsional vibration at natural frequency is completely suppressed, the torsional vibration caused by the changes in wind speed is further strengthened. This indicates the value of K_D must be appropriate for the conventional control method. Hence, K_D should be equal to 8.5×10^4 in the following simulation test.

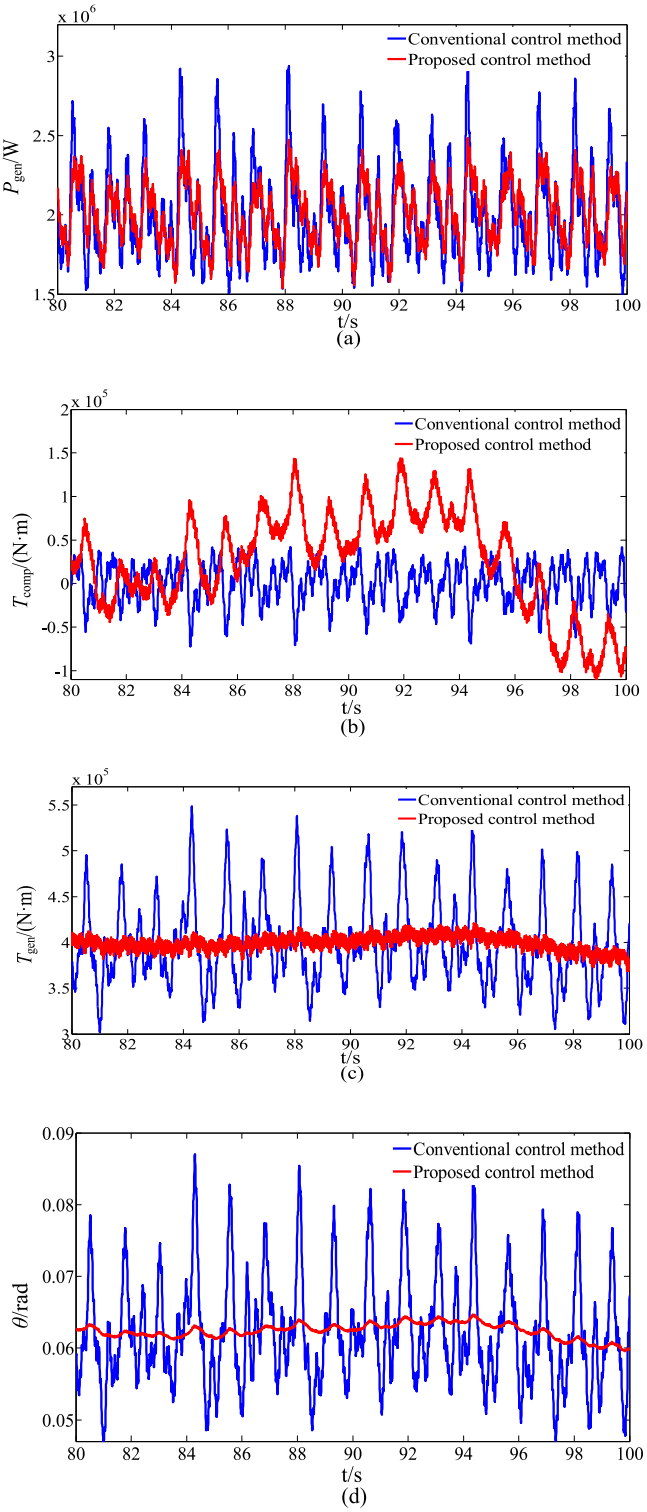

Fig. 23. System responses: (a) Power curves, (b) Compensation torque curves, (c) Electromagnetic torque curves, (d) Torsion angle curves.

$$A=\begin{pmatrix} -\frac{1}{\tau_\beta} & 0 & 0 & 0 & 0 & 0 & 0 \\ \frac{a}{J_{tur}} & -D\left(\frac{1}{J_{tur}}+\frac{1}{J_{gen}}\right) & -k_s\left(\frac{1}{J_{tur}}+\frac{1}{J_{gen}}\right) & \frac{b}{J_{tur}} & 0 & \frac{1}{J_{gen}} & 0 \\ 0 & 1 & 0 & 0 & 0 & 0 & 0 \\ \frac{a}{J_{tur}} & -\frac{D}{J_{tur}} & -\frac{k_s}{J_{tur}} & \frac{b}{J_{tur}} & 0 & 0 & 0 \\ 0 & \frac{D}{J_{gen}} & \frac{k_s}{J_{gen}} & 0 & 0 & -\frac{1}{J_{gen}} & 0 \\ 0 & 0 & 0 & 0 & 0 & 0 & 1 \\ 0 & 0 & \frac{-k_p k_s \overline{T}_{gen}}{\tau_T J_{gen}} & \frac{-k_p D \overline{T}_{gen}}{\tau_T J_{gen}} & \frac{\left(k_p D - k_i J_{gen}\right)\overline{T}_{gen}}{\tau_T J_{gen}} & \frac{k_p \overline{T}_{gen} - k_i J_{gen}\overline{\omega}}{\tau_T J_{gen}} & \frac{-\left(1+k_p\overline{\omega}\right)}{\tau_T} \end{pmatrix}$$

$$B=\begin{pmatrix} 0 \\ c/J_{tur} \\ 0 \\ c/J_{tur} \\ 0 \\ 0 \\ 0 \end{pmatrix};\ O(X,u)=\begin{pmatrix} 0 \\ o(x_1,x_2,u)/J_{tur} \\ 0 \\ o(x_1,x_2,u)/J_{tur} \\ 0 \\ 0 \\ g(X) \end{pmatrix};\ \begin{cases} g(X)=-\frac{k_p}{\tau_T J_{gen}}(x_5x_7+Dx_4x_6- \\ Dx_5x_6+k_sx_3x_6-x_6^2)-\frac{k_i}{\tau_T}x_5x_6 \\ u=\widetilde{v} \end{cases}$$

Box I.

Under these conditions, the simulation results of two control methods comparisons are shown in Fig. 23. First of all, the generator power, under this two control methods, is shown in Fig. 23(a). It is clear that the generator power is limited to the rated power 2 MW. However, compared with the conventional control method, the power fluctuation under proposed control method is smaller. In the second place, Fig. 23(b) and (c) show the compensation torque curves and electromagnetic torque curves. From Fig. 23(b) and (c), we can see that the compensating torque T_{comp} in steady state is almost zero-mean and the total torque T_{gen} which is the superposition of T_{comp} and the power controller output, also fluctuates around the rated torque. However, the electromagnetic torque under proposed method is very smooth and steady. Finally, the smoothness of electromagnetic torque can reduce the torsional vibration of drive chain shown in Fig. 23(d).

6. Conclusion

In this paper, we have firstly analyzed the small signal stability of PMSG-based WECS based on the CMT and pointed out if the system is unstable, the unstable torsion vibration of flexible drive chain could be induced. Besides, the mechanism and reasons of the torsional vibration were deeply illustrated.

First of all, the study in this paper found that the damping of drive chain is important for the system stability. And the injection of electrical damping can improve the system stability margin in the case of inadequate inherent mechanical damping. Not only that, the injecting damping also can be conducive to suppress the high-frequency forced vibration. For instance, the injected electrical damping must be over 400, the system could become stable under the system and control parameters given in this paper (see Fig. 13). For suppressing the high-frequency forced vibration in $\omega_0 = 100$ rad/s, the suppression ability with $k_D = 4\times10^5$ increased 3.5 times, compared the suppression ability with $k_D = 8.5\times10^4$ (see Fig. 14).

In the second place, with the further research about the torsional vibration, it has been found that when the damping increases to a certain extent, continuously increasing damping is still beneficial to suppress the high-frequency forced vibration, but the suppression of the low-frequency forced vibration is useless. At this time, if damping and stiffness are simultaneously injected, the suppression ability to suppress both the low-frequency and high-frequency forced vibration could be evidently improved. And the suppression ability has increased 6 times and 1 times respectively (see Fig. 14).

Thirdly, the superiority of proposed method has been further verified by comparing with the conventional method. The suppression ability of proposed method also increased about 12 times for the torsional vibration at intermediate and low frequencies, compared with the conventional method.

Eventually, the correctness and effectiveness of our analysis have been verified by the simulation experiments. The future work is to study the torsional vibration problem under other control modes (i.e., MPPT control and constant speed control) and propose more effective suppression strategies.

Appendix

WECS Parameters: Blade radius R is 31 (m). Air density ρ is 1.225 (kg m^3). Rotational inertia of wind turbine J_{tur} is 2×10^4 (kg m^2). Rated wind speed is 14 (m/s). Maximum wind power coefficient C_{Pmax} is 0.48. Optimal tip-speed-ratio λ_{opt} is 8. Inertia time constant of pitch actuator τ_β is 5. Stiffness coefficient of the drive chain k_s is 6.4×10^6 (N m s/rad). Inherent damping of the drive chain D is 10. Motor pole pairs n_p is 102. Stator resistance R_s is 0.11 (Ω). Stator inductance L_d and L_q are 0.835 (mH). Permanent magnet flux linkage Ψ is 1.25 (Wb). Rate speed ω_N is 5 (rad/s). Rate torque T_N is 4×10^5 (N m). Rotational inertia of generator J_{gen} is 700 (kg m^2) Matrices A and B are given in Box I.

References

[1] Novaes Menezes Eduardo Jose, et al. A review on wind turbine control and its associated methods. J Cleaner Prod 2018;174:945–53.
[2] Peng Li, et al. Multi-objective sizing optimization for island microgrids using triangular aggregation model and levy-harmony algorithm. IEEE Trans Ind Inf 2017;PP(99). 1-1.

[3] Peng Li, et al. Storage aided system property enhancing and hybrid robust smoothing for large-scale PV systems. IEEE Trans Smart Grid 2016;PP(99). 1-1.
[4] Wei He, Ge SS. Vibration control of a nonuniform wind turbine tower via disturbance observer. IEEE/ASME Trans Mechatronics 2015;20(1):237–44.
[5] Dongran Song. Maximum power extraction for wind turbines through a novel yaw control solution using predicted wind directions. Energy Convers Manage 2018;157:587–99.
[6] Song, et al. Power extraction efficiency optimization of horizontal-axis wind turbines through optimizing control parameters of yaw control systems using an intelligent method. Appl Energy 2018;224:267–79.
[7] Khaouch Z, et al. Mechatronic modeling of a 750kW fixed-speed wind energy conversion system using the Bond Graph Approach. ISA Trans 2016;65:418–36.
[8] Jianhu Yan, et al. Improved sliding mode model reference adaptive system speed observer for fuzzy control of direct-drive permanent magnet synchronous generator wind power generation system. IET Renew Power Gener 2013;7(1):28–35.
[9] Venkata Yaramasu, et al. High-power wind energy conversion systems: State-of-the-art and emerging technologies. Proc IEEE 2015;103(5):740–88.
[10] Bossanyi EA. The design of closed loop controllers for wind turbines. Wind Energy 2000;3(3):149–63.
[11] Bossanyi EA. Wind turbine control for load reduction. Wind Energy 2003;6(3):229–44.
[12] Zhang F, Leithead WE, Anaya-Lara O. A combined controller design of power system stabilizer and wind turbine drive-train damping filter. In: Proc. int. conf. sustainable power generation supply. 2012, p. 1–6.
[13] Licari J, Ugalde-Loo CE, Ekanayake JB, Jenkins N. Damping of torsional vibrations in a variable-speed wind turbine. IEEE Trans Energy Convers 2013;28(1):172–80.
[14] Hansen Anca D, Gabriele Michalke. Modelling and control of variable-speed multi-pole permanent magnet synchronous generator wind turbine. Wind Energy 2008;11(5):537–54.
[15] Teresa Orlowska-Kowalska, Szabat Krzysztof. Damping of torsional vibrations in two-mass system using adaptive sliding neuro-fuzzy approach. IEEE Trans Ind Inf 2008;4(1):47–57.
[16] John Licari, et al. Damping of torsional vibrations in a variable-speed wind turbine. IEEE Trans Energy Convers 2013;28(1):172–80.
[17] Roman Muszynski, Deskur Jan. Damping of torsional vibrations in high-dynamic industrial drives. IEEE Trans Ind Electron 2010;57(2):544–52.
[18] Lorenzo-Bonache Alberto, Honrubia-Escribano Andrés, Jiménez-Buendía Francisco, et al. Generic type 3 wind turbine model based on IEC61400-27-1: Parameter analysis and transient response under voltage dips. Energies 2017;10:1441.
[19] Hua Geng, Xu Dewei. Stability analysis and improvements for variable-speed multipole permanent magnet synchronous generator-based wind energy conversion system. IEEE Trans Sustainable Energy 2011;2(4):459–67.
[20] Jiawei Chen, Chen Jie, Gong Chunying. On optimizing the aerodynamic load acting on the turbine shaft of PMSG-based direct-drive wind energy conversion system. IEEE Trans Ind Electron 2014;61(8):4022–31.
[21] Fateh Farina, White Warren N, Gruenbacher Don. Torsional vibrations mitigation in the drivetrain of DFIG-based grid-connected wind turbine. IEEE Trans Ind Appl 2017;53(6):5760–7.
[22] Girsang IP, Dhupia JS, Muljadi E, Singh M, Jonkman J. Modeling and control to mitigate resonant load in variable-speed wind turbine drivetrain. IEEE J Emerg Sel Top Power Electron 2013;1(4):277–86.
[23] Teresa Orlowska-Kowalska, Szabat Krzysztof. Neural-network application for mechanical variables estimation of a two-mass drive system. IEEE Trans Ind Electron 2007;54(3):1352–64.
[24] Krzysztof Szabat, Orlowska-Kowalska Teresa. Performance improvement of industrial drives with mechanical elasticity using nonlinear adaptive Kalman filter. IEEE Trans Ind Electron 2008;55(3):1075–84.
[25] Thomsen S, Hoffmann Nils, Wilhelm Fuchs Friedrich. PI control, PI-based state space control, and model-based predictive control for drive systems with elastically coupled loads—a comparative study. IEEE Trans Ind Electron 2011;58(8):3647–57.
[26] Thomsen S, Fuchs FW. Speed control of torsional drive systems with backlash. In: Proc. EPE. Barcelona, Spain; 2009, p. 1–10.
[27] Shengquan Li, et al. On the rejection of internal and external disturbances in a wind energy conversion system with direct-driven PMSG. ISA Trans 2016;61:95–103.
[28] Lluís Trilla, Bianchi Fernando D, Gomis-Bellmunt Oriol. Linear parameter-varying control of permanent magnet synchronous generators for wind power systems. IET Power Electron 2014;7(3):692–704.
[29] Zhou F, Liu Jun. Pitch controller design of wind turbine based on nonlinear PI/PD control. Shock Vib 2018;2018:7859510, 14 pages.
[30] Khalil Hassan K. Noninear systems. New Jersey: Prentice-Hall; 1996, p. 305–7, 2.5, 5-1.